PERGAMON

International Journal of Heat and Mass Transfer 44 (2001) 4277–4285

International Journal of HEAT and MASS TRANSFER

www.elsevier.com/locate/ijhmt

Heat- and mass-transfer analysis for the condensing film flow along a vertical grooved tube

I.S. Park, D.H. Choi *

Department of Mechanical Engineering, Korea Advanced Institute of Science and Technology, Taejon 305-701, South Korea

Received 14 June 2000; received in revised form 24 January 2001

Abstract

A three-dimensional heat-transfer analysis procedure for the coupled condensing/evaporating films flowing down along the outer/inner walls of a vertical grooved tube has been developed. It is quite complex as many important solution elements such as the free-surface tracking, the conjugate heat transfer, and the phase change, need to be carefully incorporated. To effectively treat the condensing flow along the grooved outer wall, where the free-surface location is yet to be determined, a general nonorthogonal moving grid technique is employed. Given the vapor properties on both sides, the fully elliptic Navier–Stokes and energy equations are solved for the temperature and velocity fields by using a SIMPLE-type finite volume method. The analysis is successful in capturing the free-surface location along with the amount of condensate and other major three-dimensional characteristics. Most of the condensation is seen to take place on the bare portion of the groove surface and that clearly demonstrates how the heat transfer is enhanced by the grooved surface. The results are presented for various groove densities and operating conditions. The optimum groove number appears to vary with the temperature difference of the two sides. The effect of the surface tension is also discussed.

1. Introduction

Grooved or fluted tubes are widely used in modern heat exchangers, as they are easy to fabricate and very effective in heat-transfer enhancement. Applications may be found in evaporators/condensers for saline water distillation, geothermal or steam-turbine power generation, and in heat pipes for thermal control.

Despite its importance and broad industrial use, the present state of the heat-transfer analysis for the grooved tube leaves much to be desired. Most of the prior work centered on the heat-transfer aspect of the analysis and left the fluid dynamics part largely untreated as these were based on assumed or simplified free-surface shape and velocity profiles[1,2]. Ayyaswamy et al. [1] investigated the flow characteristics – mean velocity and cross-sectional area, etc., under the assumption that the radius of curvature of the free surface remains unchanged. Stephan et al. [2] calculated the radial heat transfer coefficient in heat pipes with open grooves. The free-surface shape was again given. A relationship between the film thickness, the mass-flow rate and the flute geometry was proposed experimentally by Somer and Özgen [3]: an estimation was made for the liquid carrying capacity of different flutes by dimensional analysis using the experimental data. Ma et al. [4] obtained the pressure drop due to the liquid–vapor frictional interaction with the assumption that the free-surface curvature was constant. All these are two-dimensional analyses performed on a cross-section for a fixed mass flow rate, in which the flow field is not given proper attention. In an actual condensation process, however, the axial variation of the film thickness or the mass-flow rate is not negligible and is often the quantity of interest to be determined. Frequently, the flooding of the condensate over the groove may occur at a very short distance and could degrade the heat-transfer performance of the tube.

The objective of the present study is to develop an accurate and robust analysis procedure for heat and mass transfer about the vertical grooved tube, in which

* Corresponding author. Tel.: +82-42-869-3018; fax: +82-42-869-3210.

E-mail address: dhchoi@mail.kaist.ac.kr (D.H. Choi).

0017-9310/01/$ - see front matter
PII: S0017-9310(01)00068-0

the condensing/evaporating film flows down along the outside/inside wall. The vapor is condensed outside and forms a thin film flow while the heat given up by the vapor is used to make the inside liquid to evaporate. The system can be found in a typical multieffect distillation plant.

The condensate increases as it flows downward: the initially bare surface becomes wet, the film thickens, and the heat transfer coefficient varies accordingly. For any procedure to be successful, the temperature field and the velocity field including the free-surface location must be solved simultaneously. This is a very complex three-dimensional free-surface flow which accompanies phase change. The system is in delicate thermal balance and the boundary conditions must be applied carefully. The wide variation in the film thickness, i.e., zero to some finite value, makes this a very formidable problem that requires an accurate free-surface tracking technique. The details of the solution procedure and the numerical results will be presented in the following sections.

2. Governing equations

A typical evaporator-condenser tube, which is used in a multieffect distillation system, is given in Fig. 1(a). The hot vapor is condensed on the grooved outside wall while the inside liquid evaporates using the heat taken from the outside vapor. The flow is periodic in the circumferential direction and it suffices to consider only half the period of a single groove; the schematic of the computational domain in which the shaded area represents the liquid film region is shown in Fig. 1(b). In the figure, ϕ denotes the half groove angle, and r_i, r_o the inner and outer radii, respectively. The outer radius r_o is defined as the mean of the distances measured from the tube center to the trough and the crest of the groove. For a three-dimensional laminar flow in the domain composed of liquid and solid regions, the governing equations of space conservation, continuity, momentum and energy, with dimensionless variables $\vec{x} = \vec{x}^*/2r_o$, $\vec{u} = \vec{u}^*/u_{ref}$, and $T = (T^* - T_L^*)/(T_H^* - T_L^*)$, may be written as:

$$\frac{d}{dt}\int_V dV - \int_S \vec{u}_g \cdot d\vec{S} = 0, \tag{1}$$

$$\frac{d}{dt}\int_V dV + \int_S (\vec{u} - \vec{u}_g) \cdot d\vec{S} = 0, \tag{2}$$

$$\frac{d}{dt}\int_V \vec{u} dV + \int_S [(\vec{u} - \vec{u}_g)\vec{u} + p\mathbf{I} - (2/Re)\,\mathbf{D}] \cdot d\vec{S} = \int_V 1/Fr\, dV, \tag{3}$$

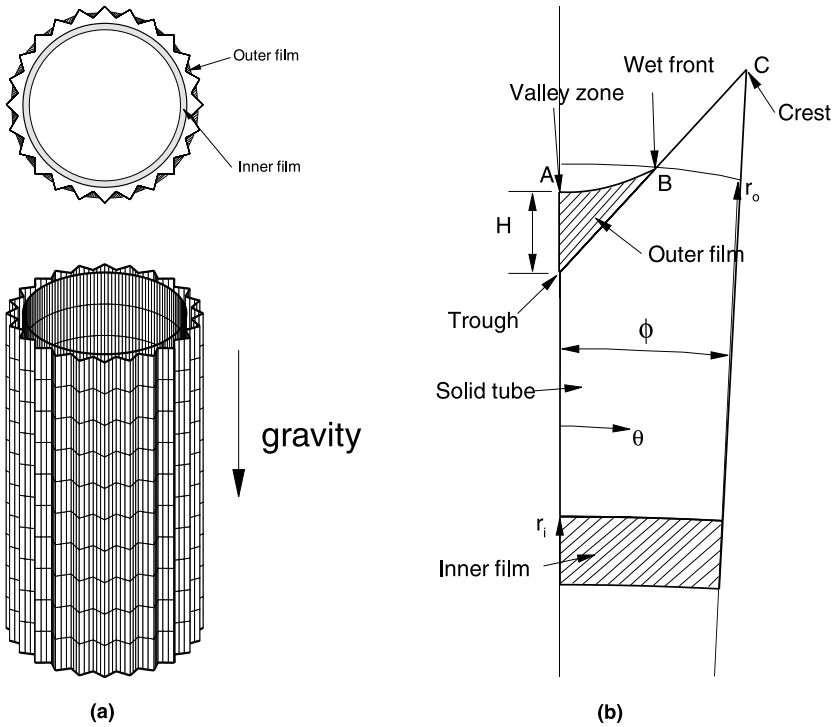

Fig. 1. Schematic of a vertical triangular grooved tube.

$$\frac{\mathrm{d}}{\mathrm{d}t}\int_V T\mathrm{d}V + \int_S [(\vec{u}-\vec{u}_g)T - 1/(Re\cdot Pr)\nabla T]\cdot \mathrm{d}\vec{S} = 0, \tag{4}$$

where $\vec{u}$ is the velocity vector, u_{ref} the reference velocity, $\vec{u}_g$ the grid velocity, p the pressure, T the temperature, and **I** and **D** the unit and rate of strain tensors, respectively. The superscript * denotes the dimensional quantity while the subscripts H and L represent the values at the outer and inner liquid–vapor interfaces, respectively. Since there is no obvious characteristic velocity in this flow, u_{ref} is conveniently given a value of unity.

The nondimensional parameters Re, Pr and Fr, i.e., the Reynolds, Prandtl and Froude numbers, are defined as $u_{ref}2r_o/\nu$, ν/α and $u_{ref}^2/(2r_o g)$, in which ν, α and g denote the kinematic viscosity, the thermal diffusivity, and the gravity, respectively. The material derivative terms in the left-hand side of the equations include the effects of the volume change due to the grid movement. The space conservation equation, Eq. (1), signifies that the volume change in any cell is equal to the volume swept by the cell boundaries [5]. Note that the governing equations reduce to a simple conduction equation in a solid wall region.

The outer film, which is formed by the condensed vapor, thickens gradually as it flows downward along, otherwise, the bare surface. To avoid the computational singularity at the inlet, where all grid lines might coalesce, the film is given a small nonzero value there. The calculation begins with an arbitrary initial free-surface shape. The final stationary location of the free surface is determined by reflecting the effects of condensation, evaporation, and the force balance between the pressure difference and the surface tension. The following boundary conditions for $\vec{u}$ and T are prescribed along the respective boundaries:

Inlet ($x=0$):

$$u_x = u_{in}(\text{uniform}), \quad u_y = u_z = 0, \quad T = 1. \tag{5}$$

Outlet ($x=L$):

$$\frac{\partial u_x}{\partial x} = \frac{\partial u_y}{\partial x} = \frac{\partial u_z}{\partial x} = \frac{\partial T}{\partial x} = 0. \tag{6}$$

Tube walls in contact with liquid:

$$u_x = u_y = u_z = 0, \tag{7a}$$

$$T, q : \text{continuous}. \tag{7b}$$

Tube walls in contact with vapor ($\overline{BC}$ in Fig. 1):

$$T = 1. \tag{8}$$

Symmetry planes:

$$\frac{\partial u_x}{\partial n} = \frac{\partial u_y}{\partial n} = \frac{\partial u_z}{\partial n} = \frac{\partial T}{\partial n} = 0. \tag{9}$$

Free surface:

$$T = 1 \text{ (outer film)}, \tag{10a}$$

$$T = 0 \text{ (inner film)}, \tag{10b}$$

$$p - p_{vapor} = -\kappa/We. \tag{10c}$$

The dimensionless parameter $We = (\rho u_{ref}^2 2r_o/\sigma)$ is the Weber number, where ρ is the density and σ the surface-tension coefficient. The curvature κ of the liquid–film free surface is defined as,

$$\kappa = \frac{\partial^2 y/\partial x^2}{[1+(\partial y/\partial x)^2]^{3/2}} + \frac{\partial^2 y/\partial z^2}{[1+(\partial y/\partial z)^2]^{3/2}}. \tag{11}$$

It seems proper to mention here that how the boundary in contact with the vapor is treated: As the vapor condenses on the bare groove surface ($\overline{BC}$ in Fig. 1), it forms an extremely thin liquid layer which is in equilibrium with the saturated steam in the vapor phase. Condition (8) states exactly that. The rate of condensate on the bare surface, and also on the film surface, is deduced from the computed normal heat flux at each time step: the heat flux equals the total latent heat given up by the condensed vapor.

The condensate on the bare groove, however, is not traced directly in the calculation since the layer it forms is too thin to be resolved by the present finite volume technique. Instead, the amount of condensate at each time step is distributed linearly across the main film surface ($\overline{AB}$ in Fig. 1), i.e., zero at the symmetry plane to an appropriate value at the wet front, in addition to the local contribution. The approximation may sound crude, but the final result after convergence should be reasonably accurate as the guessed shape is continuously modified with iteration to satisfy the free-surface boundary conditions Eqs. (10c) and (12).

Fitting the liquid–film and the tube-wall regions by a colocated general nonorthogonal grid, the SIMPLE-based finite volume method [6] is extended to obtain the steady-state solution of Eqs. (1)–(4). Since the flow is unidirectional in the streamwise direction, the upwind scheme is adopted to discretize the convective terms for simplicity. The process is iterative and the solution is considered to have converged when the sum of the residual over the entire domain in each equation becomes less than 10^{-5}.

3. Free-surface tracking

Three different approaches are currently in use for tracking the free-surface location: these are MAC, VOF and the moving grid technique. The merits and drawbacks of each method are discussed, for example, in [7]. To capture the free surface of a very thin film, whose variation is minute, the moving-grid scheme in which the

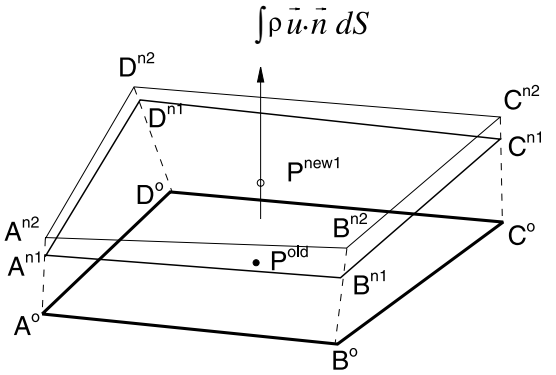

Fig. 2. The movement of surface cell node.

grid surface moves with the free surface appears most appropriate and is adopted. The typical conditions imposed on the free surface are the dynamic and the kinematic conditions. The former is the force balance between the pressure and the surface tension as is given in Eq. (10c). The latter, which says that a particle on the free surface remains to constitute the free surface, may be written as,

$$\dot{m}/\rho = \int_s (\vec{u} - \vec{u}_g) \cdot \hat{n}\, dS = \int_s \vec{u} \cdot \hat{n}\, dS - \Omega_{fs} \tag{12}$$

Here $\dot{m}$ represents the mass-transfer rate, i.e., condensation ($\dot{m}_c$) or evaporation ($\dot{m}_e$), at the freesurface boundary, and Ω_{fs} is the rate of volume swept by the free-surface cell face (volume of $A^{\circ}B^{\circ}C^{\circ}D^{\circ}A^{n1}B^{n1}C^{n1}D^{n1}$ in Fig. 2) due to the grid movement. Since $\dot{m}$ and Ω_{fs} are not known a priori, Eq. (12) normally is not satisfied in the early stage of the iterative cycle of each time step. To make the iteration converge, the difference in $\dot{m}/\rho$ before and after each iteration (volume of $A^{n1}B^{n1}C^{n1}D^{n1}A^{n2}B^{n2}C^{n2}D^{n2}$ in Fig. 2) is added to Ω_{fs}, and the corresponding grid is regenerated. The velocity and temperature fields are then calculated again in the new flow domain. The process is repeated until the free-surface cell point P (Fig. 2) stays within the specified limit. Marching in the time direction, calculation continues until the steady state is reached. It is proper to mention here that, as our primary interest lies in the condensing flow outside, the liquid film flow on the inner wall is assumed to be in the wave-free regime.

4. Results and discussions

Before getting into the complete heat-transfer analysis, the free-surface tracking aspect of the flow solver is verified against the fully developed flow data [3] taken from a vertical fluted tube. Starting with a rather arbitrary inlet condition, the calculation is performed for a sufficiently long streamwise computational domain ($20r_o$) so that the unique fully-developed state is reached within the domain. The maximum film thickness (H, see Fig. 1) over the groove for various flow rates is compared in Fig. 3. The agreement is excellent and confirms that the code is sufficiently accurate in locating the free-surface shape.

The next step is to check the performance of the procedure for the case with heat and mass transfer. The average condensation heat-transfer coefficient for R113 on a grooved surface is compared with the experimental data in Fig. 4. The heat-transfer coefficient h vs. the temperature difference between the trough and the free surface is plotted. The tube of 50 mm long has the groove of half period 2° and the depth 0.87 mm. It is seen from the figure that, by using a grooved tube, the heat transfer can be enhanced by 5–10 times over the Nusselt solution for a flat plate. The present result shown in the figure is in excellent agreement with the data. Also compared in the figure is the semi-analytic solution of Mori et al. [8] who approximated the free surface as an arc of uniform radius with an assumed contact angle. Although their results appear to follow the general trend, the agreement deteriorates as the temperature difference becomes small.

A series of calculations is then carried out for various cases. The total number of grooves (N) around the tube

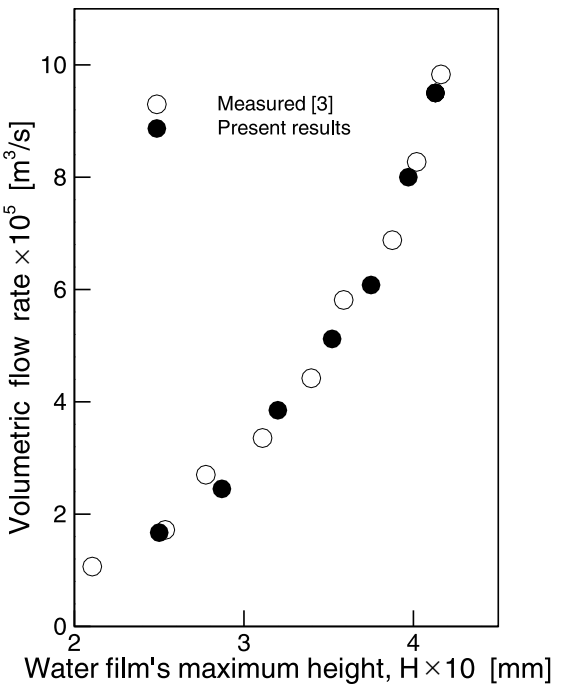

Fig. 3. Maximum film thickness with respect to the volumetric flow rate.

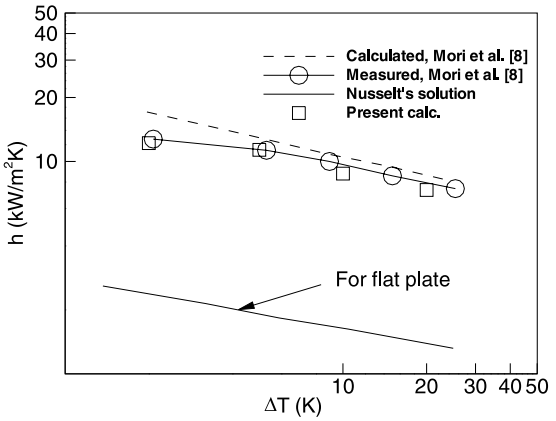

Fig. 4. The condensation heat transfer coefficient vs. ΔT for a vertical grooved surface [8].

is varied to be 30, 40, and 60. The corresponding half period of a groove ϕ becomes 6°, 4.5°, and 3°, respectively. The groove depth, the inner and outer tube diameters are kept constant for all calculations: 1.5, 45, and 50 mm. The tube is made of brass (70% Cu, 30% Zn) and the liquid is pure water. With the saturated vapor condition, three different temperature settings, i.e., the temperature difference (ΔT) between the inner and outer vapors of 5°C, 10°C, and 20°C, are examined.

The calculation for the outer film begins with a crude initial guess: a very thin film with flat surface. The thickness of the inner film at the inlet and the associated nondimensional mass flow rate, $(2r_o)^2 \cdot \int_A u^* dA/u_{ref}$, are fixed at 0.5 mm and 0.18. Fig. 5 shows a typical grid at the end of the calculation, and hence describes the final converged free-surface shape. Here, the regions of outer film, tube wall, and inner film are fitted by grids of $(150 \times 30 \times 30)$, $(150 \times 10 \times 45)$, and $(150 \times 10 \times 30)$, respectively. The grid is stretched to place more grids near the wall and the free surface; the streamwise grid distribution is uniform, however.

The free-surface level rises with accumulating condensate. The level and the shape of the free surface at various streamwise sections for $N = 40$ and $\Delta T = 10$ are presented in Fig. 6. As the flow develops, the film thickness increases due to condensation, and the effects of surface tension drive the free surface to take a concave shape. The results obtained with two other grid distributions, i.e., $(100 \times 15 \times 15)$ and $(100 \times 20 \times 20)$, are also compared in the figure to see the grid dependency of the solution. The surface profiles at $x = 4/5L$ for the two denser grids show little difference and therefore substantiates that the $(150 \times 30 \times 30)$ grid is sufficient in capturing the details of the flow field.

The concave shape of the free surface is due to the combined effects of the boundary-layer development and the surface tension. As the fluid in the central region travels faster than that near the wall, the film gets

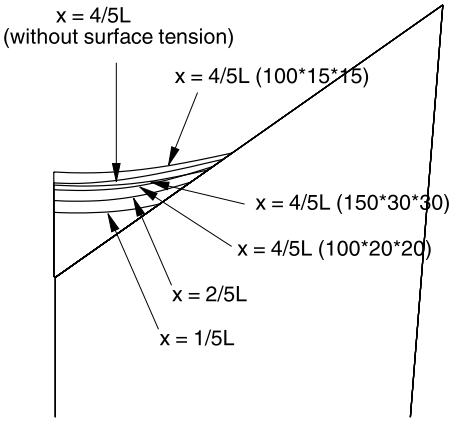

Fig. 6. Free-surface shapes at various axial stations for $N = 40$.

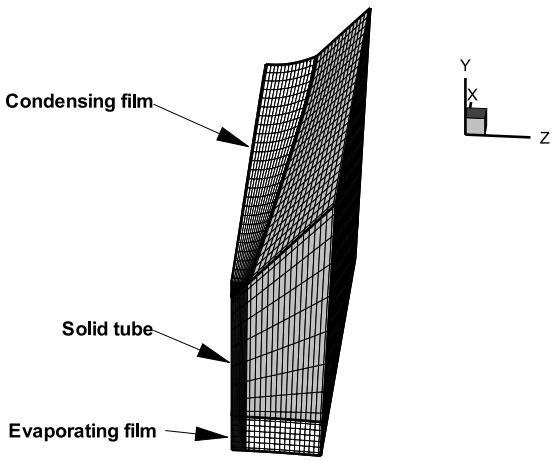

Fig. 5. A typical grid system for computation.

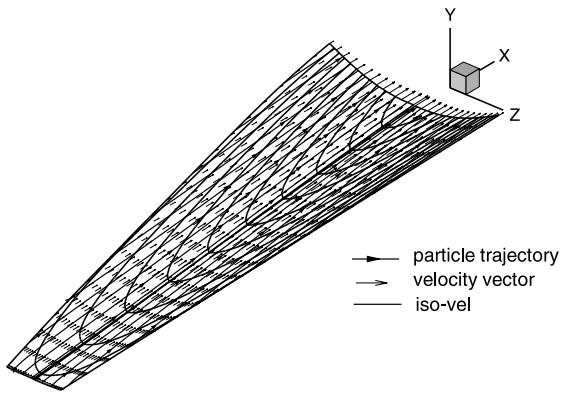

Fig. 7. Particle trajectory, axial velocity contour, and vector plot on the outer film free surface for $N = 40$.

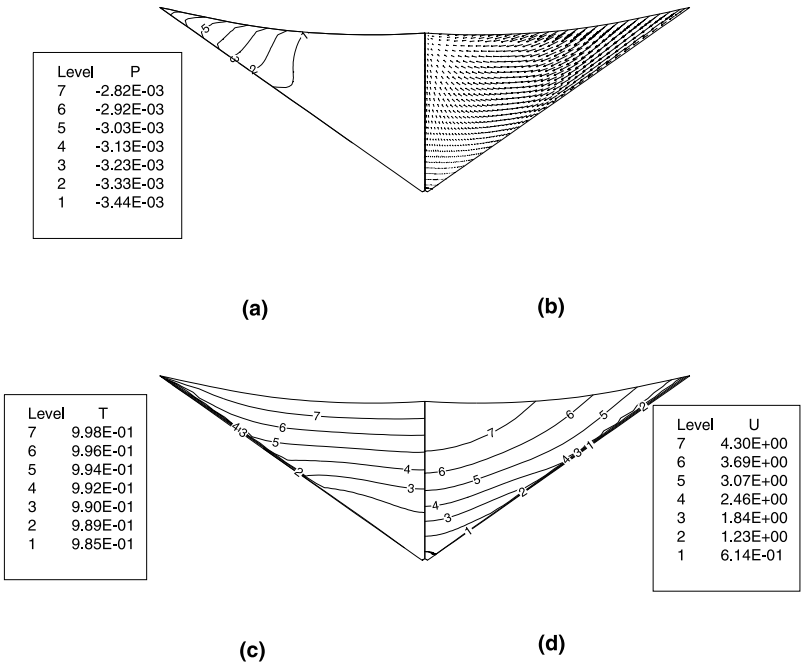

Fig. 8. Cross-sectional flow field at $x = 4/5L$ for $N = 40$: (a) isobars; (b) vector plot; (c) isotherms; (d) axial velocity contour.

thinner in the middle and also drags the fluid from the side. This is well illustrated in the next two figures, Figs. 7 and 8(b). Fig. 7 shows the trajectory of fluid particles and the axial isovels on the surface. The surface fluid particle moves inward and the axial velocity increases as the flow proceeds downstream. The accelerating axial velocity signifies the increasing flow rate due to condensation. As the direction of the gravity is perpendicular to the free-surface normal, it is not obvious what the surface tension would do. To see how this affects the flow field, we repeated the calculation with the surface tension effects out. The resulting surface profile at the cross-section $x = 4/5L$ is compared in Fig. 6. The film without the surface-tension effects seems to be slightly thicker and more concave than the other. The total condensate is correspondingly larger as tabulated in Table 1. A notable difference between the two may be the strong secondary motion driven by the pressure gradient seen in the case with the surface-tension effects (Fig. 8(b)).

The flow and temperature pattern in a typical streamwise cross-section is depicted in Fig. 8. The pressure field (Fig. 8(a)) indicates that the pressure is highest at the wet front and decreases gradually towards the middle. The small inward pressure gradient drives the fluid to move from the crest to the valley of the groove as is seen in the vector plot of the secondary flow in Fig. 8(b). Although it is not shown in the paper, such inward pressure gradient is absent in the case without the surface tension effects and the secondary flow is almost nonexistent as mentioned above. It is interesting to note that the secondary motion, which is generally weak compared to the axial velocity, is most active near the film surface closer to the wet front. This inward motion makes the fluid in the middle move faster axially as is shown in Fig. 8(d). The temperature field presented in Fig. 8(c) suggests that most of the heat transfer is through the thin part of the film and we will come back to this point later. Fig. 9 shows the temperature fields at various axial stations for the same case. The isotherms

Table 1
Nondimensional flow rate per unit azimuthal angle for various groove numbers

N	30	40	60
$\Delta T = 10$	0.500×10^{-4}	0.515×10^{-4}	0.493×10^{-4}
$\Delta T = 10$ (without surface tension)		0.520×10^{-4}	
$\Delta T = 20$	0.765×10^{-4}	0.108×10^{-3}	Flood
$\Delta T = 5$	0.294×10^{-4}	0.277×10^{-4}	0.222×10^{-4}

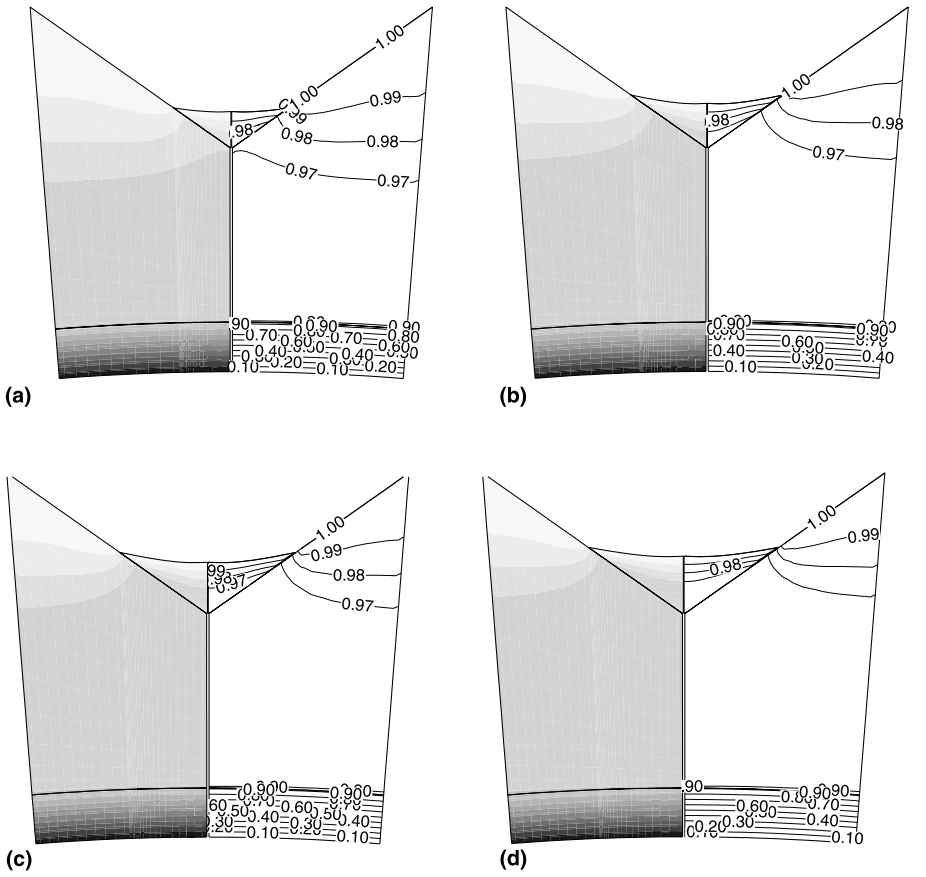

Fig. 9. The isotherms on various cross-sections for $N = 40$: (a) $x = 1/5L$; (b) $x = 2/5L$; (c) $x = 3/5L$; (d) $x = 4/5L$.

for the inner film region indicate that both the flow and temperature distributions are nearly axisymmetric. The three-dimensionality is confined mostly in the outer part of the groove. Because of high conductivity of the solid, the temperature of the tube wall quickly becomes fairly uniform. The temperature variation is largest in the vicinity of the wet front and incurs the highest heat transfer there.

The phenomenon is better illustrated in Fig. 10, which shows the local heat flux along the surface in

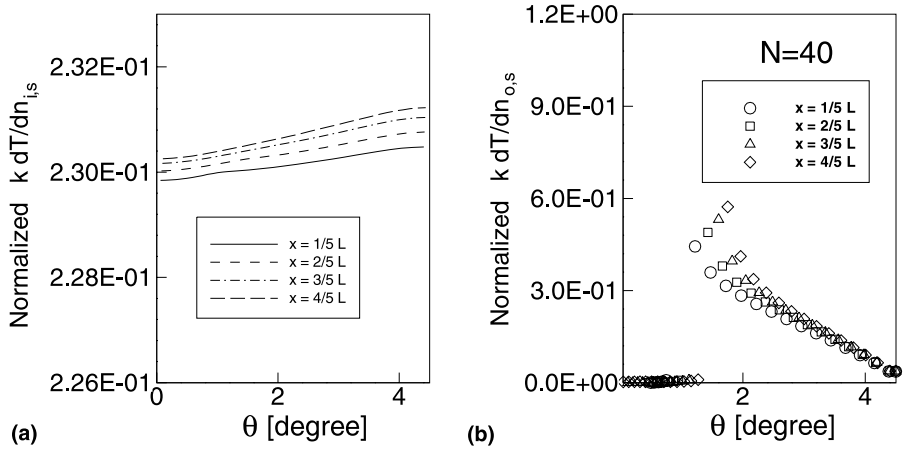

Fig. 10. The local heat flux distribution normalized by the cross-sectional total heat flux at various stations: (a) inner film; (b) outer film.

contact with the vapor, i.e., the film free surface and the bare groove surface. The local heat flux at various cross-sections, which is normalized by the total sum of each cross section, is presented in the figure. Evidently the flux in the bare groove region accounts for most of the heat transfer of the cross section. The heat transfer through the film surface, on the other hand, is fairly insignificant and demonstrates why the grooved tube is effective in heat-transfer enhancement. As the film flow develops, the bare portion of the groove decreases with the rising film level; the maximum heat flux is seen to increase to compensate for the reduction in effective heat-transfer area. The trend in the crest neighborhood is unaffected, however. It is interesting to note that the highest heat flux is observed at the wet front where the shortest heat path is realized. These characteristics remain unchanged as the number of grooves around the tube is varied. The heat flux through the free surface of the inner-film flow is also plotted at the respective cross sections. The distribution is much more uniform than that on the outer surface. The three-dimensionality is still observed as the heat flux is larger in the portion opposite to the bare groove region outside.

Finally, the cumulative condensate at the end of the calculation domain is compared in Table 1. The nondimensional condensate per unit azimuthal angle is shown for the groove numbers of 30, 40, and 60, and the temperature difference between the inside and outside vapors of 5°C, 10°C, and 20°C. The nondimensional condensate is defined as

$$\dot{m}_c = \frac{\int_S (k/h_c) \cdot (\mathrm{d}T^*/\mathrm{d}n)\,\mathrm{d}S}{\phi \rho u_{\mathrm{ref}} 4 r_o^2}, \tag{13}$$

where k is the thermal conductivity and h_c the latent heat. It is seen from the table that the amount of condensate increases with the groove number when ΔT is 20 while the opposite is true when ΔT is 5. Interestingly, for $\Delta T = 10$, the maximum occurs when the groove number is 40. For $N = 60$ and $\Delta T = 20$, the film flow covers the groove completely to the crest at some location and the calculation is aborted. Although the code can be modified readily to handle the case, no attempt was made to do so.

The results suggest that the optimum groove number, which delivers the maximum condensate, is not uniquely determined but dependent upon the temperature difference. As the temperature difference becomes small, so does the amount of condensate and N_{opt} decreases. Increasing the groove number beyond this optimum value actually has the adverse affects on the heat-transfer enhancement. This maybe elaborated as follows: when the amount of condensate is small, the film occupies very small area near the valley where the frictional resistance is high. The friction retards the flow and the thickening film gets to cover more of the groove surface. This reduces the effective heat transfer area and hinders the condensation. On the other hand, when the film becomes thick as in the case of large ΔT, the flow is less affected by the presence of the wall and therefore the condensate tends to increase with N. The result is intriguing and can be usefully incorporated in the design process of the grooved tube for a given operating condition. The optimum groove number, shape, and where to put runoff disks along the tube to prevent flooding may be a few of many design parameters that may be determined by the present analysis.

5. Conclusions

The evaporation and condensation processes for the films flowing down along the inner and outer walls of a vertical triangular grooved tube have been investigated. Given the vapor properties on both sides, the liquid regions and the tube wall are solved in a fully coupled manner. The Navier–Stokes procedure that incorporates the moving-grid technique is successful in predicting the free-surface profile, and the comprehensive flow and temperature fields. The surface tension induces strong secondary flow and therefore tends to make the film temperature more uniform. Calculations for various groove densities and thermal operating conditions reveal that the optimal groove number that delivers the maximum condensate varies with the temperature differential of the two sides. The procedure can be quite useful in fixing the design parameters such as the groove number, the groove shape, and also the spacing of the runoff disk that breaks up the film flow.

Acknowledgements

This work was supported by Korea Institute of Machinery and Metals. Partial support was also provided by the Ministry of Education under the BK21 Project in the later stages of the study.

References

[1] P.S. Ayyaswamy, I. Catton, D.K. Edwards, Capillary flow in triangular grooves, J. Appl. Mech. 41 (1974) 332–336.
[2] P.C. Stephan, C.A. Busse, Analysis of the heat transfer coefficient of grooved heat pipe evaporator walls, Int. J. Heat Mass Transfer 35 (1992) 383–391.
[3] T.G. Somer, C. Özgen, Hydrodynamics of condensate films on fluted tube surfaces, Part I, Desalination 34 (1980) 233–247.
[4] H.B. Ma, G.P. Peterson, X.J. Lu, The influence of vapor–liquid interactions on the liquid pressure drop in triangular

microgrooves, Int. J. Heat Mass Transfer 37 (1994) 2211–2219.
[5] I. Demirdžić, M. Perić, Space conservation law in finite volume calculations of fluid flow, Int. J. Numer. Meth. Fluids 8 (1988) 1037–1050.
[6] S.V. Patankar, Numerical Heat Transfer and Fluid Flow, McGraw-Hill, New York, 1980.
[7] J.L. Thé, A time implicit method for the solution of fluid flow problems with moving boundary, Ph.D. Thesis, University of Waterloo, Canada, 1993.
[8] Y. Mori, K. Hijikata, S. Hirasawa, W. Nakayama, Optimized performance of condensers with outside condensing surfaces, J. Heat Transfer 103 (1981) 96–102.